

Observation of charge screening in semiconductor nanocrystals

R. L. MacDonald

Department of Physics, Brown University, Providence, Rhode Island 02912

N. M. Lawandy

Department of Physics and Division of Engineering, Brown University, Providence, Rhode Island 02912

(Received 31 August 1992)

Charge screening in semiconductor nanocrystals is observed using a technique based on the optical erasure of optically encoded second-harmonic generation in semiconductor microcrystallite-doped glasses. The optical erasure rate for illumination above the band gap ($\hbar\omega > E_g$) is dominated by the recombination of charges trapped outside the nanocrystals with photogenerated free carriers. The measured erasure rate is found to decrease with increasing intensity at photogenerated carrier concentrations which correspond to screening lengths of the order of the crystallite diameter. Rate calculations based on the recombination of electrons, trapped outside the crystallite, with quantized hole states, perturbed by a screened electric field, correctly predict the observed behavior.

I. INTRODUCTION

Semiconductor microcrystallite-doped glass (SDG), a solid solution of nanometer-sized semiconductor spheres within a host glass, provides a unique environment to study collective electronic effects in confined systems. These systems can be made with an average crystallite radius comparable to and even smaller than the bulk exciton radius, leading to quantization of the translational energy of the exciton. In this regime, decreasing the crystallite radius increases the energy of the excited electronic states, an effect that has been observed in the absorption spectra of SDG.¹⁻³ The small crystallite size (~ 100 Å diam) and long recombination time⁴ (~ 2 μsec) result in large densities of free carriers for relatively small amounts of excitation. Theories have been put forward that predict a blueshift of the absorption edge and modification of the nonlinear optical properties of SDG due to charge screening,^{5,6} but so far only absorption saturation measurements have shown indications of carrier screening effects.⁶ In order to more directly study the effects of charge screening in these systems we use a technique based on optically encoded second-harmonic generation in SDG.⁷ The second-harmonic generation (SHG), which is normally absent due to inversion symmetry in a random medium, results in second-harmonic intensities nine orders of magnitude larger than predicted from interface, electric quadrupole, and magnetic dipole effects,⁸ and thus provides a sensitive measurement of the symmetry-breaking process in the material.⁹

The material encoding process, which results from simultaneous exposure to intense radiation at the fundamental and second-harmonic frequencies [$E(\omega)$ and $E(2\omega)$], changes the glass both microscopically and macroscopically such that it efficiently frequency doubles the light at ω . Although this effect has been seen in fibers made from homogeneous glass,^{10,11} the microscopic mechanism in those systems remains unsolved.¹² One of the initial models for optical encoding in glass was based

upon optical rectification via the third-order nonlinear coefficient $\chi^{(3)}(0; -\omega, -\omega, 2\omega)$.¹¹ The model proposed that exposure of the glass to $E(\omega)$ and $E(2\omega)$ results in a dc electric field that oscillates along the length of the encoding beam,

$$E_{dc} \propto \chi^{(3)}(0; -\omega, -\omega, 2\omega)[E^*(\omega)]^2 E(2\omega) e^{-i\Delta kz}, \quad (1)$$

where $\Delta k = 2k(\omega) - k(2\omega)$, and $k(\omega)$ and $k(2\omega)$ are the wave vectors of the fundamental and second-harmonic waves in the material, respectively. When this dc electric field is frozen into the material, second-harmonic generation occurs via the nonlinear optical coefficient $\chi^{(3)}(-2\omega; \omega, \omega, 0)$. Since the second-harmonic field grows as

$$\frac{dE(2\omega)}{dz} \propto \chi^{(3)}(-2\omega; \omega, \omega, 0)[E(\omega)]^2 E_{dc} e^{i\Delta kz}, \quad (2)$$

the oscillation of E_{dc} is just right to phase match the process, which is described by an effective $\chi^{(2)} = \chi^{(3)}(-2\omega; \omega, \omega, 0)E_{dc}$. While a dc electric field greater than 10^6 V/m has been measured in encoded homogeneous glass optical fibers,¹³ the above model cannot explain the effect in homogeneous glasses. This is due to the small value of $\chi^{(3)}$ in glasses at optical frequencies, which results in dc electric fields four orders of magnitude smaller than required to explain the observed SHG. Even if a large enough electric field could be produced, the mechanism for encoding this in homogeneous glass has not been explained due to the negligible photoconductivity at the wavelengths used.

The $\chi^{(3)}$ encoding picture described above can be realized using glasses embedded with semiconductor microcrystallites. Such systems possess large free-carrier mobility and nonlinear optical coefficients within the semiconductor nanocrystals, and an abundance of traps at the semiconductor-glass interface, making them ideal for encoding electric fields. The proposed encoding mechanism in SDG,⁷ schematically shown in Fig. 1, is described by the following steps: (1) free carriers are generated by absorption of the second harmonic; (2) the dc field, result-

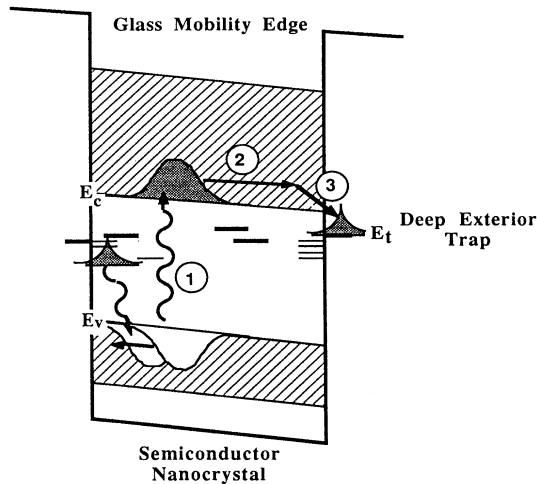


FIG. 1. Proposed mechanism for optical encoding in SDG as described in the text.

ing from the semiconductor's resonance enhanced $\chi^{(3)}(0; \omega, \omega, -2\omega)$, sweeps the electrons to one side of the crystallite; (3) the electrons are trapped in long-lived traps within the surrounding glass, leaving behind a semi-permanent electric field. These traps are not the same as those responsible for microsecond recombination and mid-band-gap luminescence, as evidenced by their extremely long lifetime (greater than months at room temperature). Electrons are believed to play the dominant role in surface trapping because the large effective mass of the holes confines them to the center of the sphere in semiconductors such as CdS.¹⁴ Previous measurements have shown that encoded SDG produces second-harmonic light with $I(2\omega) \propto I(\omega)^2$, that $I(2\omega)$ grows with length, that the encoding occurs only for SDG with a semiconductor band gap near the second harmonic ($E_g \sim 2\hbar\omega$),⁷ and that the tensor properties of the encoded $\chi^{(2)}$ are consistent with SHG generated by an electric field within the crystallites.¹⁵ In addition, $\chi^{(2)}$ can be erased by heating the encoded spot above 65 °C or by exposing it to focused laser radiation. The thermal erasure has been shown to be consistent with trap depths ~ 0.65 eV below the conduction-band edge,⁷ and is supported by luminescence measurements in similar SDG.¹⁶

Since the large SHG signals in semiconductor microcrystallite-doped glass are a direct measure of the internal dc field, the process of erasure by photogeneration of carriers can be effectively used to study charge screening in the semiconductor microcrystallites. The experimental work we will describe is based on optical erasure of the encoded electric field using photon energies both above and below the semiconductor band gap to show that free-carrier effects dominate in the erasure process for $\hbar\omega > E_g$, and that screening effects can be observed in the intensity dependence of the erasure rates in this regime.

II. OPTICAL ERASURE BELOW THE SEMICONDUCTOR ABSORPTION EDGE

All experiments were performed on 3-mm-thick samples of Schott OG530 glass, which contains microcrystal-

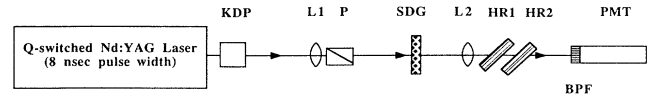


FIG. 2. Experimental setup for optical encoding and erasure measurements. KDP, doubling crystal; L1, L2; lens (25-cm focal length); P, polarizer, SDG, sample; HR1, HR2, high reflectors at 1064 nm; BPF, bandpass filter at 532 nm; PMT, photomultiplier tube.

lites of $\text{CdS}_{0.9}\text{Se}_{0.1}$ ($\hbar c/E_g \sim 515$ nm). These samples were encoded for SHG using linearly polarized 1064- and 532-nm light from a Q-switched (20-Hz, 8-nsec pulses) frequency-doubled Nd:YAG laser (Fig. 2). The resulting SHG was detected by removing 532-nm light from the encoding beam and measuring the 532-nm light produced after the sample with a photomultiplier tube. The SHG was found to grow more than five orders of magnitude above the initial reading. After ~ 30 min the encoding reached steady state, as evidenced by unchanging SHG readings. The encode-erase cycle could be repeated many times (> 5) on the same spot, indicating that the dc field is removed by draining trapped electrons rather than by filling long-lived traps on the opposite side of the nanocrystal.

Sub-band-gap erasure was used to determine the erasure rate due to direct photoionization of the trapped electrons. The encoded spots were illuminated in 5-min intervals by radiation from a cw model-locked (76-MHz, 2-ps pulse duration) dye laser (Rhodamine 6G and DCM) with wavelengths from 559 to 669 nm. The SHG was measured after each interval, and erasure rates, Γ , were determined by fitting the data to a decaying exponential. The resulting erasure rates are of the order of 2×10^{-5} $\text{cm}^2/\text{W sec}$ and increase linearly with intensity (Fig. 3). In addition Γ was found to vary by a factor of only 3 over all wavelengths studied. This slow wavelength dependence is consistent with optical excitation of the trapped electrons to the nanocrystal conduction band, a process which exhibits weak wavelength dependence over a wide range of photon energies, extending to wavelengths well above the band gap. This is based on photoionization of

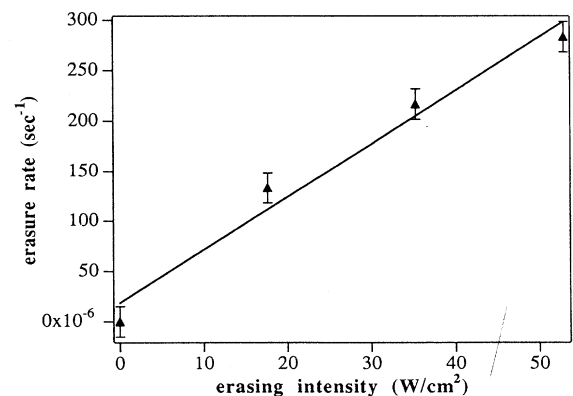


FIG. 3. Sub-band-gap optical erasure rate vs intensity ($\lambda = 640$ nm).

trapped electrons in bulk semiconductors, which has slow dependence on photon energy, for energies greater than the trap depth.¹⁷

Since the slow dependence of photoionization rates on wavelength holds for bulk semiconductors we tested for analogous behavior in semiconductor nanocrystals. This was done by calculating the cross sections and ionization rates from δ -function traps, located both inside and outside of the nanocrystal, to excited states of a three-dimension (3D) spherical infinite well potential. For traps located in the center of the well, the trapped electron's wave function is $(\alpha/2\pi)^{1/2}e^{-\alpha r}/r$ where α determines the trap size, and is given by $\alpha=(2m_e E_i/\hbar^2)^{1/2}$, for an electron with effective mass m_e in a trap of depth E_i . For example, luminescent traps in SDG are known to have a distribution of depths centered around 0.7 eV below the conduction band, which leads to $\alpha^{-1}\sim 5 \text{ \AA}$. The effective-mass approximation, which has been shown to be applicable to SDG with crystallites containing only 100 atoms,¹⁸ is used to describe the motion of electrons and holes in the semiconductor nanocrystal. The conduction-band envelope wave function for a particle in a spherical well of radius R is

$$\Psi_c(\mathbf{r}) = A_{nlm} Y_l^m(\Omega) j_l(k_{ln}), \quad (3a)$$

where

$$A_{nlm}^2 = \frac{2}{R^3 [j_l'(k_{ln}R)]^2}, \quad (3b)$$

$Y_l^m(\Omega)$ is a spherical harmonic and $j_l(x)$ is the l th order spherical Bessel function with its n th zero at $x=k_{ln}R$. The matrix element, M_{ic} , for an optical transition between the trap state and a conduction-band state is

$$|M_{ic}|^2 = \left(\frac{eA}{m_e} \right)^2 \frac{4\alpha}{3R^3} \frac{1}{[k_{ln}j_l'(k_{ln}R)]^2} \frac{1}{[1+(\alpha k_{ln})^2]^2}, \quad (4)$$

where e is the electron charge, A is the vector potential of the optical field, and transitions are only allowed to the $l=1$ states by conservation of angular momentum. The overall transition rate, calculated using this matrix element and summing over energy-conserving final states, yields a photoionization rate, for wavelengths well above the ionization energy ($\hbar\omega > E_i$), six orders of magnitude larger than the observed sub-band-gap erasure rates. When the traps are not in the center of the spherical well, exact calculations of the matrix element become prohibitively difficult, but the matrix element can be calculated numerically. For traps inside the crystallite the photoionization rates, calculated using a 3D numerical integration routine to find M_{ic} , were more than four orders of magnitude too large. If the trap is moved $\sim 10 \text{ \AA}$ outside the crystallite and its wave function is taken to be an s -state with a 3- \AA radius (the small trap size is chosen to be consistent with the large band gap of the surrounding glass), the order of magnitude of numerically calculated ionization rates agrees with measurements and exhibits the observed slow wavelength dependence. Based on this,

we believe that optical erasure for $\hbar\omega < E_g$ is consistent with photoionization of electrons *trapped outside the crystallite*. This indicates that the long-lived traps required for encoding are external to the semiconductor nanocrystal. The existence of such external traps explains the slow optical erasure as well as the long decay times of the encoded $\chi^{(2)}$ grating at ambient temperatures. Evidence for external trapping of electrons in SDG exposed to above band-gap light has been found using thermally stimulated luminescence results.¹⁹ In addition, experiments on photodarkening of SDG are consistent with photoejection of electrons from nanocrystals and population of external traps.^{20,21}

III. OPTICAL ERASURE ABOVE THE SEMICONDUCTOR ABSORPTION EDGE

Erasure rates for $\hbar\omega > E_g$ were ~ 500 times larger than for $\hbar\omega < E_g$ with the equivalent intensities, indicating that free carriers, and not photoionization of traps, play an important role in the rapid erasure. Since the electrons in the conduction band of the semiconductor microcrystallites trap in picoseconds, the holes are believed to play the dominant role in above-band-gap erasure. The intensity dependence of the erasure process was measured using cw radiation from an argon-ion laser ($\lambda=514.5 \text{ nm}$) on OG530 glass encoded by the previously described procedure. Erasure rates, Γ , were determined by fitting measurements of SHG versus exposure time to an exponential, with SHG measurements taken every 10 sec. The results (Fig. 4) show that Γ decreases with increasing intensity over the range 6–12 W/cm^2 , corresponding to an average of ten electron-hole pairs per crystallite and a classical Debye screening length comparable to the crystallite radius. This unexpected feature can be explained by considering charge screening effects on the erasure process. Note that, even for the largest intensities used, the contribution of direct photoionization to the erasure rate, as described in the preceding section, is negligible.

The above-band-gap erasure process appears to be

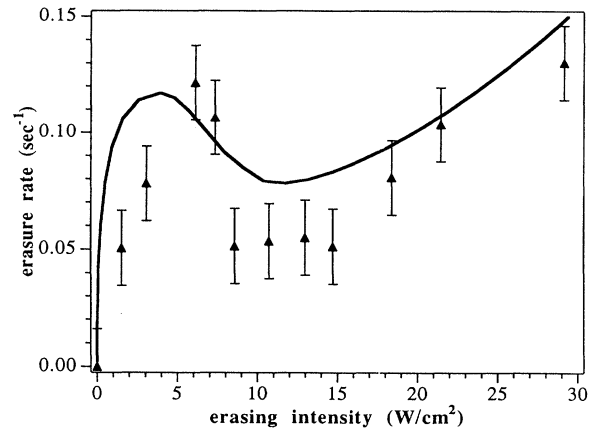


FIG. 4. Optical erasure rate vs intensity for strongly absorbed light ($\lambda=514.5 \text{ nm}$). The triangles are measured rates and the solid line is the calculated intensity dependence.

dominated by direct recombination of the externally trapped electron with photogenerated holes. The electric field from the trapped electrons, which is responsible for the SHG process, pulls the holes towards the electrons, resulting in recombination and a decreased electric field. For large excitation rates (high intensities) charge screening becomes important, and the effective field seen by each hole is reduced. This reduces the overlap of wave functions between the trapped electron and each hole in the valence band, and hence a reduced recombination rate per hole. Thus, to explain the above-band-gap erasure process at high intensities, charge screening must be taken into account. Plasma screening in bulk semiconductors has been modeled using a quantum-mechanical Green's-function theory²² and using linear-response theory for the many-particle Hamiltonian of the system with a phenomenological Yukawa potential.⁵ The second approach yields a closed form solution, whereby electrons and holes in the plasma interact through a screened Coulomb potential,

$$V_s(r) = -e \frac{\exp(-\kappa r)}{\epsilon_0 r}, \quad (5)$$

where κ is the inverse screening length and

$$\kappa^2 = \frac{8\pi e^2}{\epsilon_0 k_B T} \sum_{\alpha} \frac{1}{(2\pi)^3} \int d\mathbf{k} f_{\alpha}(\mathbf{k}) [1 - f_{\alpha}(\mathbf{k})], \quad (6a)$$

$$f_{\alpha}(\mathbf{k}) = \frac{1}{\exp[E_{\alpha}(\mathbf{k}) - \mu_{\alpha}] + 1}, \quad (6b)$$

and

$$E_{\alpha}(\mathbf{k}) = \frac{\hbar^2 k^2}{2m_{\alpha}} + \frac{E_g^0}{2}. \quad (6c)$$

This approach leads to a relative motion of electrons and holes governed by a Schrödinger equation with $V = V_s(r)$.

The screening mechanism in SDG is complicated by the confined geometry and by surface traps at the semiconductor-glass interface. Free-carrier densities where the screening length becomes comparable to the nanocrystal diameter are of the order of 10^{17} cm^{-3} , corresponding to 0.13 holes per 50-Å radius nanocrystal, so screening cannot be viewed as a many-body effect in this regime. The screening, which most likely occurs via directional electron trapping, can, however, be viewed in the ergodic limit, which is applicable to the erasure process because of the large ratio of erasure time to recombination time ($t_{\text{erase}}/t_{\text{recomb}} \sim 10^7$). When an electron-hole pair is created in the encoded nanocrystal, the dc field influences where the electron will trap via $e^{-U(\Omega)/kT}$, where $U(\Omega)$ is the time-averaged electrostatic potential energy on the surface of the nanocrystal (Ω is a coordinate on the 2D crystallite surface) due to the dc field from the externally trapped electron. Since the electric field is essentially time independent, the screening should be the same as for free-carrier screening where the carriers are constrained to a 2D surface. The hole wave function will now be perturbed by the potential due to both trapped electrons. For example, if the trapped electrons are on

opposite sides of the nanocrystal, which is the most energetically favorable position, then the hole will experience a zero net field and will not be pulled towards the externally trapped electron. Finally, the electron which is trapped in a short-lived trap will recombine with the hole in microseconds, and this cycle continues millions of times, on average, before the externally trapped electron recombines with one of the holes, justifying the statistical treatment of the trapping process. For higher intensities, where multiple photogenerated carrier pairs are likely to exist in each nanocrystal, the field from the externally trapped electron gradually washes out due to other trapped electrons and to the screening by the valence-band holes, i.e., $\bar{U}(\Omega)$ becomes a constant, and screening due to the many valence-band holes becomes important. The end result is that the screening process in SDG should depend on carrier population in a manner similar to that in bulk semiconductors, even for small average free-carrier occupation numbers.

IV. MODEL FOR ABOVE-BAND-GAP ERASURE

To determine if screening effects as described above could significantly affect the optical erasure rate in our experimental system, we modeled the erasure process, taking charge screening into account. The wave functions for valence-band holes were numerically calculated using the shooting method for a particle in a one-dimensional box with infinite walls and under the influence of a screened Coulomb potential. Accounting for finite penetration of hole states into the glass did not change our results. We calculated the overlap integral between a trapped electron, whose size and position were determined from sub-band-gap erasure experiments, and the lowest-energy valence-band hole to determine the recombination rate per hole. The recombination rate per hole was multiplied by the number of valence-band holes to give the recombination rate for a given inverse screening length $\Gamma(\kappa)$. For high excitations (> 10 holes per nanocrystal), where many holes are in large angular momentum states, the overlap between the trapped electron and free hole wave functions will no longer be close to that of the lowest excited state hole. We accounted for this by multiplying $\Gamma(\kappa)$ by the average square overlap of all occupied 3D spherical box states (no dc electric field since $\kappa R > 5$) with the trapped electron's wave function.

Since the experiments determine the erasure rate as a function of intensity, I , we need to relate I to the hole density and to the related screening parameter κ . Equation (6a) results in $\kappa^2 \propto p_1$, the classical Debye screening result, where p_1 is the population of valence-band holes. To find the relationship between p_1 and intensity we model the nanocrystal optical excitation cycle using a three level system, as is commonly done in analysis of photoluminescence and absorption saturation results.^{4,16} The three energy levels with significant population are the valence band (subscript 1), conducting band (subscript 3), and trap states (subscript 2). The rate equations governing population dynamics of the three levels, under the influence of an excitation of intensity I , are expressed as

$$\frac{dn_3}{dt} = BI - \gamma_2 n_3 (n_2^T - n_2) - \gamma_3 n_3 p_1, \quad (7a)$$

$$\frac{dn_2}{dt} = \gamma_2 n_3 (n_2^T - n_2) - \gamma_1 n_2 p_1, \quad (7b)$$

$$n_3 + n_2 = p_1, \quad (7c)$$

where I is the illumination intensity, B is the Einstein coefficient for photon absorption, n_3 is the population of conduction-band electrons, n_2 is the population of trapped electrons, n_2^T is the total number of electron traps, and γ_i are the relaxation rate constants between the various states (Fig. 5). The steady-state solution of the rate equations yields

$$BI = \gamma_2 (n_2^T)^2 \left\{ [(1-\delta)P_1 - 1] + (A^2 + \delta P_1)^{1/2} \right\} \\ \times \left\{ A \left[1 + \left(1 + \frac{4\delta P_1}{A^2} \right)^{1/2} \right] + \beta P_1 \right\}, \quad (8a)$$

$$A = \frac{1 - (1+\delta)P_1}{2}, \quad (8b)$$

where $\delta = \gamma_1/\gamma_2 \ll 1$, $\beta = \gamma_3/\gamma_2 \ll 1$, and $P_1 = p_1/n_2^T$. The result is that I varies as $P_1^2 \propto \kappa^4$ until $n_2 = n_2^T$, after which I varies as $P_1 \propto \kappa^2$. This allows the calculated erasure rates, $\Gamma(\kappa)$, to be converted to $\Gamma(I)$ and compared with the measured rates.

Values for parameters used in the calculations were taken from published results. The energy of the system was scaled to $\hbar^2/2m_h R^2$, where m_h is the hole effective mass $\sim 0.8m_0$,²³ and R is the crystallite radius $\sim 50 \text{ \AA}$.²⁴ The electric field maximum was taken to be 10^8 V/m , based on the second-harmonic generation efficiencies observed in Ref. 7. The decay constants, γ_i , between the various states were taken to be consistent with photoluminescence studies.⁴ The total number of recombination traps was taken to correspond to trap population saturation at $I(514.5 \text{ nm}) = 5 \text{ W/cm}^2$ or 10^7 photogenerated carrier pairs per nanocrystal per second, consistent with luminescence⁴ and phase conjugating experiments.²⁵ Thus the only free parameter in the problem is the scaling of rate with calculated recombination probability, i.e., the height of the curve. The resulting curve (Fig. 4) fits the measured data remarkably well considering the one-dimensional approximation used, which is not surprising since the solid angle that results in most of the overlap between trap and free hole is small (< 0.004). Initially the recombination rate grows with intensity, as the probability of finding a hole in the valence band increases and

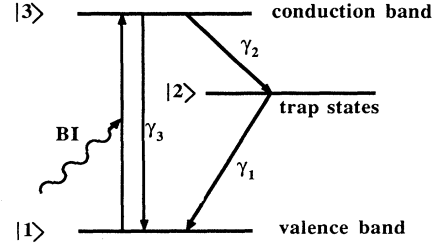


FIG. 5. Energy-level diagram for free-carrier population dynamics.

the attraction towards the externally trapped electron is strong. The recombination rate per hole, however, is decreasing due to the increasing number of trapped electrons and hole-hole interactions, which screen the Coulomb field from the externally trapped electron. This results in an overall recombination rate which actually decreases with increasing hole density over a small range. Eventually the screening effect saturates, and the rate increases with hole density again, due to direct statistics as well as the filling of higher angular momentum states having larger wave-function overlap with the externally trapped electron.

V. CONCLUSION

In conclusion, we have used the technique of optical erasure of optically encoded second-harmonic generation in SDG to observe charge screening in nanometer-sized semiconductor crystals. The encoding leaves behind a semipermanent dc electric field within the semiconductor nanocrystals, whose strength is determined by SHG. Below-band-gap optical erasure measurements indicate that this process is dominated by photoionization of electrons trapped outside the microcrystallite. Above-band-gap optical erasure of the encoded field is found to be dominated by the recombination of free carriers with externally trapped charges, and the measured intensity dependence of this effect is reproduced by calculations based on recombination of electrons in long-lived traps with photogenerated holes, including the effect of a screened dc electric field. Future work will extend these measurements to the quantum dot regime, where quantum confinement plays an even more dramatic role.

ACKNOWLEDGMENTS

This work was supported by the U.S. Air Force Office of Scientific Research. R.M. would also like to thank the National Science Foundation and the IBM Corporation for financial support. The authors thank Professor A. Houghton for useful discussions.

¹A.I. L. Efros and A. L. Efros, *Fiz. Tekh. Poluprovodn.* **16**, 1209 (1982) [*Sov. Phys. Semicond.* **16**, 772 (1982)].

²A. I. Ekimov and A. A. Onushchenko, *Fiz. Tekh. Poluprovodn.* **16**, 1215 (1982) [*Sov. Phys. Semicond.* **16**, 775 (1982)].

³A. I. Ekimov and A. A. Onushchenko, *Pis'ma Zh. Eksp. Teor. Fiz.* **40**, 337 (1984) [*JETP Lett.* **40**, 1136 (1984)].

⁴M. Tomita, T. Matsumoto, and M. Matuoka, *J. Opt. Soc. Am. B*, **5**, 165 (1989).

⁵L. Banyai and S. W. Koch, *Phys. Rev. Lett.* **57**, 2722 (1986).

⁶G. R. Olbright, N. Peyghambarian, S. W. Koch, and L. Banyai, *Opt. Lett.* **12**, 413 (1987).

⁷N. M. Lawandy and R. L. MacDonald, *J. Opt. Soc. Am. B* **8**, 1307 (1991).

⁸R. W. Terhune and D. A. Weinberger, *J. Opt. Soc. Am. B* **4**, 661 (1987).

⁹N. M. Lawandy, *Phys. Rev. Lett.* **65**, 1745 (1990).

- ¹⁰U. Österberg and W. Margulis, *Opt. Lett.* **11**, 516 (1986).
- ¹¹R. Stolen and H. W. K. Tom, *Opt. Lett.* **12**, 505 (1987).
- ¹²N. M. Lawandy, in *Proceedings of the International Workshop on Photoinduced Self-Organization Effects in Optical Fiber*, edited by Francois Ouellette [*Proc. SPIE* **1516**, 99 (1992)].
- ¹³A. Kamal *et al.* (unpublished).
- ¹⁴A. I. Ekimov *et al.*, *Solid State Commun.* **69**, 565 (1989).
- ¹⁵R. L. MacDonald and N. M. Lawandy, *Electron. Lett.* **27**, 2331 (1991).
- ¹⁶M. K. Kull and J.-L. Coutaz, *J. Opt. Soc. Am. B* **7**, 1963 (1990).
- ¹⁷G. Lucovsky, *Solid State Commun.* **3**, 299 (1965).
- ¹⁸Z. W. Fu and J. D. Dow, *Bull. Am. Phys. Soc.* **32**, 557 (1986).
- ¹⁹V. Ya. Grabovskis, Ya. Ya. Dzenis, A. I. Ekimov, I. A. Kudryavstev, M. N. Tolstoi, and U. T. Rogulis, *Fiz. Tverd. Tela (Leningrad)* **31**, 272 (1989) [*Sov. Phys. Solid State* **31**, 149 (1989)].
- ²⁰J. Malhotra, D. J. Hagan, and B. G. Potter, *J. Opt. Soc. Am. B* **8**, 1531 (1991).
- ²¹M. Tomita and M. Matsuoka, *J. Opt. Soc. Am. B* **7**, 1198 (1990).
- ²²See, for example, H. Haug and S. Schmitt-Rink, *Prog. Quantum Electron.* **9**, 3 (1984); H. Haug, *J. Lumin.* **30**, 171 (1985).
- ²³L. E. Brus, *J. Chem. Phys.* **79**, 5566 (1983).
- ²⁴V. Degiorgio, G. Banfi, G. Righini, and A. Rennie, *Appl. Phys. Lett.* **57**, 2879 (1990).
- ²⁵B. VanWanterghem, S. M. Saltiel, T. E. Dutton, and P. M. Rentzepis, *J. Appl. Phys.* **66**, 4935 (1989).